Conference Proceedings

EuroSun 2016
Palma de Mallorca (Spain), 11 - 14 October 2016

A numerical model to evaluate the flow distribution in large solar collector fields in different operating conditions

Federico Bava, Janne Dragsted and Simon Furbo

DTU Civil Engineering, Technical University of Denmark, Kgs. Lyngby (Denmark)

Abstract

A numerical model to evaluate the flow distribution in a large solar collector field was developed in Matlab and is presented in this study. Model and measurements from a solar collector field were compared and a good agreement was found. The model was then used to study the flow distribution in different array layouts. Balancing valves proved to be an effective way to achieve uniform flow distribution also in conditions different from those for which the valves were regulated, as well as in case of irregular layouts with different compositions of the collector rows. A Tichelmann connection gave a uniform flow distribution, especially if the distribution pipe diameter is reduced so to give a constant pressure drop gradient. The reduction in power output from the collector field was approximately proportional to the square of the root-mean-square deviation of the flow distribution, but was generally small, at least under the considered assumptions.

Keywords: *solar collector, solar collector field, flow balancing, flow distribution, parallel connection.*

1. Introduction

1.1. Background

An increasing number of large scale solar collector fields have been built in Europe in the last years. Of the total collector area installed at the end of 2014, 77% was located in Denmark (Mauthner et al., 2016). The development in this country has been driven by specific factors, such as high taxation on fossil fuels and widespread use of district heating (DH), to which large collector areas can be connected (Furbo et al., 2015). More than 800,000 m^2 of collector fields were installed in Denmark at the end of 2015 and this number is expected to grow in the next future (Mauthner et al., 2016). Also the size of the collector fields has been increasing. The current largest field in Vojens has a collector area of 70,000 m^2 (Mauthner et al., 2016), but by the end of 2016 a 150,000 m^2 collector field should be completed in Silkeborg (EnergySupply, 2016).

The larger the collector fields and the higher the number of collector rows, the larger the risk of non-uniform flow distribution. Non-uniform flow distribution cause non-uniform temperature distribution across the collector field, so decreasing the thermal performance. The negative effect of flow maldistribution on the thermal performance was investigated by Chiou (1982), who treated this effect in a single collector with parallel channels. He presents a method to determine how much the collector efficiency is penalized by the flow maldistribution. Defined a *flow nonuniformity parameter* as the root mean square deviation of the channels flow rates, he concludes that the deterioration of the collector efficiency is proportional to the 1.8^{th}-1.9^{th} power of such parameter. Wang and Wu (1990) presented a model to calculate the flow distribution in collector arrays with vertical pipes, both in U- and Z-configuration. The U-configuration presents a higher maldistribution than the Z-configuration. Fan et al. (2007) investigated through CFD calculations the flow and temperature distribution in a large collector for solar assisted DH plants. Model results and measurements are compared. The authors conclude that the flow distribution is driven by friction (and so buoyancy can be neglected), if the velocity in the collector pipes is high compared to the temperature rise across the collector. Bava and Furbo (2015) propose a numerical model to calculate the pressure drop and flow distribution in a U-type harp collector. Based on the conclusions of Fan et al. (2007), the authors argue

doi:10.18086/eurosun.2016.05.05 Available at http://proceedings.ises.org

that in large collector fields for DH applications the relation between the fluid velocity in the absorber pipes and the temperature rise in the collector is such that buoyancy can be neglected. The model was compared against measurements carried out on a collector for solar assisted DH plants and good agreement was found.

Ideally, the layout of a collector array should be with short pipe lengths and uniform flow distribution. Though, it is not possible to optimize both these aspects simultaneously, so a compromise must be found. Rohde and Knoll (1976) analyzed different options to minimize the flow maldistribution in a collector field of 12 rows connected in parallel. The options included various size manifolds, manifold area changes, different locations of the inlets and exits to the manifolds, orifices and balancing valves. The last two are presented as the best solutions, both in terms of performance and cost. It is observed that a specific configuration of valve settings maintains the desired flow distribution only at a specific total flow rate. The topic of flow distribution in collector fields is also treated by Knabl et al. (2014). Maintaining a constant and large diameter in the distribution pipes or adopting a Tichelmann configuration (Fig. 6.b) improves the flow distribution. However, both options have higher costs due to the longer/larger pipes. Balancing valves are another possibility, but these increase the cost, installation time and maintenance (in case of defective valves). A cheaper solution is to install differently sized pipes in the collector rows, but the hydraulic design must be calculated in advance and very precisely, as a later adjustment would be very expensive.

In Danish solar collector fields, the pipe diameter of the distribution pipes is progressively reduced, as fluid is diverted to the collector rows. Balancing valves are then installed in each row to obtain a uniform flow distribution. These are regulated to achieve the desired flow distribution in full-load conditions (high flow rate, high solar radiation, nominal inlet/outlet temperatures), so that the outlet temperature from all rows is the same. This is done by supplying the different rows with flow rates proportional to the collector row area.

1.2. Sizing distribution pipes and balancing valves in solar collector fields: HySelect software

The design of the hydraulic network of a solar collector array can be a time-consuming and cumbersome procedure to be carried out manually. Hence, software able to carry out the same task can be extremely useful, making the job of planners and designers much easier. A program which can be used for this purpose is the commercial software *HySelect* from IMI Hydronic Engineering (IMI Hydronic, 2014). The software can be used to design and balance generic hydraulic networks, and so solar collector fields as well, in terms of pipe size, pump head, types and settings of balancing valves. The software returns the valve type and valve settings which should be applied to achieve a user-defined flow distribution. Additionally, it makes easy to optimize the pipe diameters (based on several pipe dimension standards) to fulfill fluid velocity or pressure gradient constraints. The software also contains built-in libraries of the thermophysical properties of a variety of fluids, including those most commonly used in solar heating systems, such as water and ethylene/propylene glycol-water mixtures. When designing a branched system, the program automatically adds and considers the pressure drop caused by the resulting tee junctions and bends. HySelect is intuitive to use and extremely fast in returning the results.

Despite these strengths, the software has some limitations. First of all, its reduced flexibility. As mentioned above, the program returns the valve setting configuration which guarantees a certain flow distribution. It does not calculate the flow distribution itself. Consequently, once a system has been balanced for specific boundary conditions (e.g. total flow rate and fluid temperature), it is not possible to analyze how the flow distribution varies, if the boundary conditions are changed. Secondly, the fluid temperature is assumed constant throughout the system. This approximation does not seem very accurate when designing solar collector fields for DH application, where the temperature rise across the collector field can be 40-50 K. Furthermore, the thermophysical properties (especially viscosity) of glycol-water mixtures are known to be strongly dependent on the temperature (see Section 2.1.2). Thirdly, complex layouts, having for example a common return pipe such as in Fig. 3, cannot be designed. Finally, the correlations used for evaluating the pressure drop in tee junctions are not in agreement with the literature (Idelchik, 1994). No reference to a literature source is provided and the used correlations are not stated in the software manual (IMI Hydronic, 2014). The difference between HySelect and Idelchik's correlations for pressure drops in tee junctions is shown in Fig. 1. The diagram was obtained assuming a distribution pipe from which 10 parallel circuits parted. The distribution pipe and the circuit pipes had diameter of 81 mm and 36 mm respectively. The system was supplied with a total flow rate of 20 $m^3 h^{-1}$, uniformly distributed in the 10 parallel circuits.

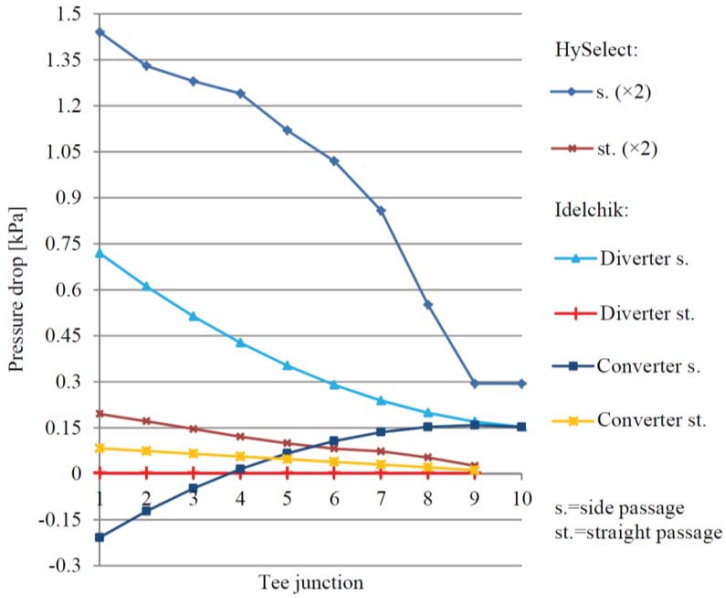

Fig. 1: Comparison between HySelect and Idelchik's correlations for pressure drop in tee junctions.

The fluid was water at 75 °C. Looking at Fig. 1, it is first of all noted that HySelect does not show the different contributions of the diverging and converging tee junctions, but only the overall pressure drop. Secondly, comparing the pressure drops in the diagram, it can be seen that for the straight passage the combined pressure drops from HySelect are approximately twice as large as the pressure drops that Idelchik's correlations give for the straight passage of the converging tee. On the other hand, the pressure drop in straight passage of the diverging tee junction predicted by Idelchik is negligible compared to that in the converging tee junction. Consequently, it could be neglected in the calculations without introducing a significant error. Regarding the side passages, the combined pressure drop from HySelect is between two and four times higher than Idelchik's pressure drop for the side passage of the diverging tee junction.

2. Material and method

2.1. Numerical model

2.1.1. Pressure drop correlations

To calculate how a fluid flow distributes in a branched system, it is necessary to know the relation between flow rate and pressure drop across each component. In fact, the fluid flow distributes in such a way that the pressure difference between two points is the same, regardless of the hydraulic path which connects one to the other. Because the relation between pressure drop and fluid velocity depends on factors such as Reynolds number, flow regime, etc., the flow distribution in a branched system may vary in different conditions.

In a collector field three main categories of hydraulic components can be identified: solar collectors, pipes and fittings (bends, tee junctions, valves, etc.).

The pressure drop characteristic of a solar collector is not always given in the technical datasheets and - even when provided - it usually refers to a specific fluid type and temperature. Different fluids and/or temperatures can affect the pressure drop. In this study the model proposed by Bava and Furbo (2016) was used to evaluate the pressure drop across each solar collectors, more specifically a HTHEATStore 35/08 from Arcon-Sunmark A/S (SP, 2016a). The HTHEATStore 35/08 is a flat plate harp collector with 18 U-connected absorber pipes. The pipes are 5.80 m long and have an inner diameter of 7.3 mm. The two manifolds are 2.24 m long and have an inner diameter of 32.9 mm. The collector gross area is 13.57 m^2 and its efficiency coefficients are η_0=0.757, a_1=2.2 W m^{-2} K^{-1} and a_2=0.007 W m^{-2} K^{-2} with respect to the collector gross area. Fig. 2 shows the modeled pressure drop for a 35% propylene glycol/water mixture, whose physical properties were evaluated through (Eq. 5) and (Eq. 7).

The friction loss along the distribution pipes was calculated by the Darcy-Weisbach equation (Eq. 1):

$$\Delta p = \lambda \frac{l}{D_h} \frac{\rho w^2}{2} \qquad \text{(Eq. 1)}$$

In (Eq. 1) Δp [Pa] denotes the pressure drop; λ [-] the Darcy friction factor; l [m] the pipe length; D_h [m] the pipe hydraulic diameter, which equals the inner diameter for a full flow circular pipe; ρ [kg m^{-3}] the fluid density and w [m s^{-1}] is the mean fluid velocity.

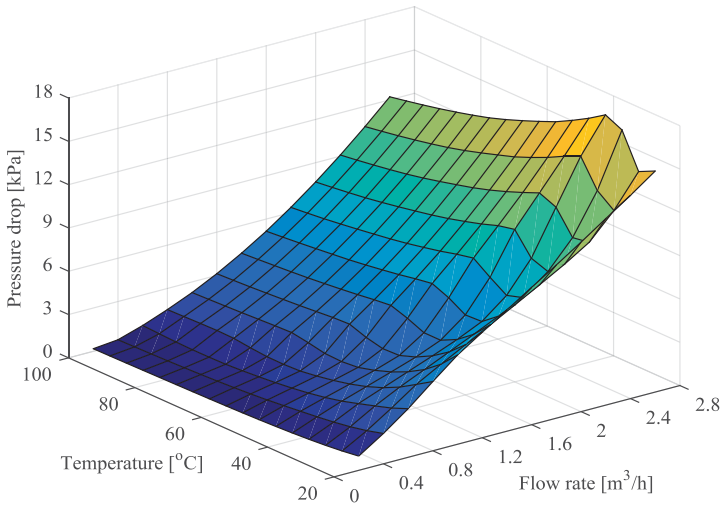

Fig. 2: Pressure drop in a HTHEATstore 35/08 collector as function of temperature and flow rate for 35% propylene glycol/water mixture.

Laminar regime was assumed for Reynolds numbers Re<2300, while turbulent regime was assumed for Re>4000 (Holman, 2002). According to the flow regime, the friction factor was calculated through the Hagen-Poiseuille law (Eq. 2) and the Haaland (1983) correlation (Eq. 3) respectively. The roughness of steel pipes was assumed to be ε=10^{-4} m. In the transition region (2300<Re<4000) the friction factor was evaluated by linearly interpolating the value obtained from (Eq. 2) at Re=2300 and that from (Eq. 3) at Re=4000.

$$\lambda = 64/Re \qquad \text{(Eq. 2)}$$

$$\lambda^{-1/2} = -1.8 \log_{10}\{[\varepsilon/(3.7\, D_h)^{1.11} + 6.9/Re]\} \qquad \text{(Eq. 3)}$$

Correlations from Idelchik (1994) were used to estimate the local losses in fittings, such as bends, tee junctions, changes of flow section area, etc. Regarding the balancing valves, the manufacturers usually provide the pressure drop characteristic as flow factor K_v (Eq. 4):

$$K_v = V \cdot [SG/(\Delta p \cdot 10^{-5})]^{1/2} \qquad \text{(Eq. 4)}$$

In (Eq. 4), V [m^3 h^{-1}] represents the volume flow rate and SG [-] the fluid specific gravity.

The flow factor is mainly function of the valve setting. However, deviations from the nominal K_v value can be expected with fluids different from water and flow rates significantly smaller than the valve nominal flow rate (IMI Hydronic, 2015). In these cases, the nominal K_v value should be corrected. In this study, valves from IMI-Hydronic were used and their corrected flow factors were evaluated through HySelect software.

2.1.2 Fluid properties

Propylene glycol/water mixtures with glycol concentration of 30-40% (Windeleff and Nielsen, 2014) are normally used as heat transfer fluid in solar assisted DH plants. In this study, the thermophysical properties of these mixtures were evaluated using the correlations proposed by Conde (2011).

$$\rho = 508.4 - 0.1824x + 965.8T^* + 0.2803xT^* - 472.2\cdot(T^*)^2 \qquad \text{(Eq. 5)}$$

$$c_p = 4476 + 608.6 - 715.0T^* - 1939xT^* + 478.7\cdot(T^*)^2 \qquad \text{(Eq. 6)}$$

$$\ln \mu = -1.028 - 0.1003x - 19.94T^* + 0.1464xT^* + 14.6205\cdot(T^*)^2 \qquad \text{(Eq. 7)}$$

When comparing the thermophysical properties of propylene glycol reported in literature (Conde, 2011; DOW, 2008; George and Sastry, 2003; Melinder, 2007), a large variability was found. So, for the model validation, a sample of propylene glycol/water mixture was taken from the collector field and its properties were determined with an Anton Paar DMA4100 densimeter and an Anton Paar AMV200 viscometer. The sample (35% glycol) was tested every 10 °C in the range 20-80 °C. The following correlations were found:

$$\rho = 1038.3 - 0.4419T - 1.940 \cdot 10^{-3} T^2 \quad \text{(Eq. 8)}$$

$$\mu = \begin{cases} -1.449 \cdot 10^{-8} T^3 + 3.066 \cdot 10^{-6} T^2 - 2.337 \cdot 10^{-4}\, T + 7.289 \cdot 10^{-3} & if\ T < 38\,°C \\ 0.1803 T^{-1.232} & if\ T > 38\,°C \end{cases} \quad \text{(Eq. 9)}$$

In (Eq. 5)-(Eq. 9), ρ [kg m^{-3}] denotes the density, c_p [J kg^{-1} K^{-1}] the specific heat, μ [Pa s] the dynamic viscosity, x [%] the mass concentration of propylene glycol in the mixture, while T^* is a factor defined as T^*=273.15/(T+273.15), where T [°C] is the fluid temperature.

2.1.3 Matlab implementation

Based on the above mentioned correlations, a numerical model was developed in Matlab, to calculate the flow distribution in a solar collector field. The layout of the collector field, the collector pressure drop, valves types and settings, dimensions of distribution pipes, fittings and the operating conditions (fluid type, field flow rate and fluid inlet temperature) need to be specified in the model. The temperature profile along the collector rows can be evaluated in two ways. The first is that a unique outlet temperature, equal for all collector rows, is defined in input and a linear temperature profile is assumed along the collector row. The second option requires the collector efficiency parameters, solar irradiance and ambient temperature. The temperature profile in each row is given by the solution of (Eq. 10), which assumes steady state conditions.

$$\dot{m}\, c_p \frac{dT}{dA} = G\, \eta_0\, K_\theta - a_1 \cdot (T - T_{amb}) - a_2 \cdot (T - T_{amb})^2 \quad \text{(Eq. 10)}$$

In (Eq. 10), $\dot{m}$ [kg s^{-1}] is the mass flow rate, A [m^2] is the gross/aperture collector area, G [W m^{-2}] is the hemispherical solar irradiance on the collector plane, η_0 [-] is the peak efficiency of the solar collector coherent with the definition of A, K_θ [-] is the incident angle modifier, a_1 [W m^{-2} K^{-1}] and a_2 [W m^{-2} K^{-2}] are the first and second order heat loss coefficients coherent with the definition of A, T [°C] is the fluid temperature and while T_{amb} [°C] is the ambient temperature.

To determine the actual distribution, the set of equations (Eq. 11) is solved iteratively. (Eq. 11) imposes both the mass conservation across the collector field (first line in (Eq. 11)) and the uniformity of pressure drop along the different hydraulic paths (from second line downward):

$$\begin{pmatrix} 1 & 1 & 1 & 1 & 1 & 1 \\ k_{1,j} \cdot \dot{m}_{1,j} & -k_{2,j} \cdot \dot{m}_{2,j} & 0 & 0 & 0 & 0 \\ 0 & k_{2,j} \cdot \dot{m}_{2,j} & -k_{3,j} \cdot \dot{m}_{3,j} & 0 & 0 & 0 \\ \vdots & \vdots & \vdots & \vdots & \vdots & \vdots \\ 0 & 0 & 0 & 0 & k_{N-1,j} \cdot \dot{m}_{N-1,j} & -k_{N,j} \cdot \dot{m}_{N,j} \end{pmatrix} \begin{pmatrix} \dot{m}_{1,j+1} \\ \dot{m}_{2,j+1} \\ \dot{m}_{3,j+1} \\ \vdots \\ \dot{m}_{N,j+1} \end{pmatrix} = \begin{pmatrix} \dot{m}_{tot} \\ 0 \\ 0 \\ \vdots \\ 0 \end{pmatrix} \quad \text{(Eq. 11)}$$

In (Eq. 11), k [kg^{-1} m^{-1}] is a hydraulic resistance coefficient; the subscripts 1, 2, ..., N denote the collector row and N is the total number collector rows; the subscript *tot* refers to the total flow rate supplied to the solar collector field and the subscript j denotes the iteration number. The factor k_i is defined so that the product $\left(k_i \cdot \dot{m}_i{}^2\right)$ represents the pressure drop along the entire i-th hydraulic path. The value of k_i takes into account both the pressure drop along the i-th collector row, proportional to the square of the row flow rate $\dot{m}_i$, and the pressure drop along the portion of distribution pipes and tees included in the i-th hydraulic path, properly normalized to the flow rate $\dot{m}_i$.

The system (Eq. 11) is iteratively solved until the maximum difference in the collector row flow rates between two consecutive iterations is lower than 0.1%.

2.2. Description of the solar collector field and experimental setup

The developed model was based on the layout of the solar collector field installed near Høje Taastrup (Denmark). The layout is shown in Fig. 3. The collector field (gross collector area of 3257 m^2) consisted of

two subfields of 12 collector rows each. The rows consisted of 10 HTHEATStore 35/08 collectors each and were 5.5 m apart from each other. Because near the collector field there was no auxiliary heating plant, the control strategy aimed at reaching an outlet temperature from the collector field which was approximately the DH supply temperature. Nominal inlet and outlet temperatures of the field were 50-55 °C and 90-95 °C respectively, and the flow rate ranged between 8 and 50 $m^3 h^{-1}$, depending on the solar irradiance.

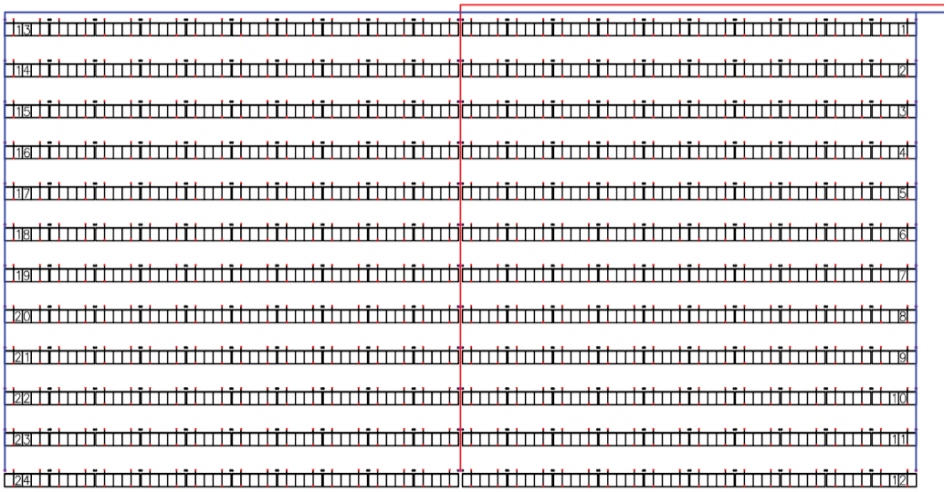

Fig. 3: Layout of Høje Taastrup solar collector field: blue and red lines represent supply and return pipes respectively (adapted from Arcon-Sunmark A/S).

The distribution pipes were made of preinsulated steel pipes. The largest inner diameter was 10.7 cm and it progressively became smaller as more fluid was diverted to the collector rows. At the inlet of each row a balancing valve was installed. In the middle of the field, the flows from each couple of row outlets were merged and then directed into the return pipe. The heat transfer fluid was a 35% propylene glycol/water mixture (Section 2.1.2).

To measure the flow distribution in the collector field, a differential pressure sensor TA-SCOPE from IMI Hydronic was used. The balancing valves have two measuring points, one before and one after the valve member. By measuring the pressure drop across the valve, the flow rate can be calculated through (Eq. 4). Specifying the type of fluid in the device, this calculates the fluid density and viscosity thanks to the built-in temperature sensor and corrects the valve flow factor. The maximum relative error when measuring the flow rate with this method is shown in Fig. 4. The error increases rapidly for low valve settings, so it is recommended to use settings higher than two. In Høje Taastrup collector field the lowest setting was 2.2.

The volume flow rate to the field was measured by an electromagnetic flow meter with accuracy of 0.5%.

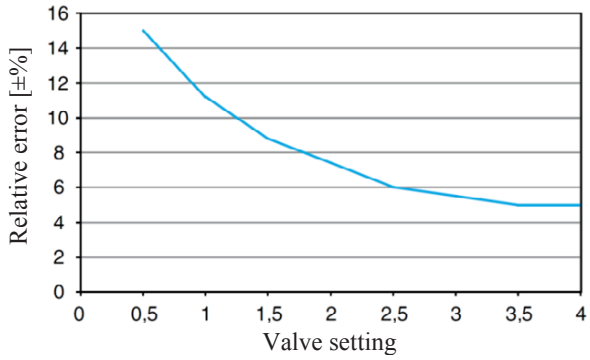

Fig. 4: Relative error on the measured flow rate across a STAD valve as function of the valve setting (IMI Hydronic, 2015).

At first, the flow distribution was measured keeping the same valve settings as in normal operation. However, the difference in the row flow rates was lower than the measurement error. Hence, the measurements were repeated after changing the setting of the first 10 valves in the eastern subfield, so to

introduce a higher maldistribution, which could be more easily detected. The flow distribution across the collector field was measured for a total flow rate of 50.3±0.3% m^3 h^{-1}. The test was carried out in a cloudy day, so that the temperature across the field was constant (45.0±1.3 °C) during the entire duration of the test.

3. Results and discussion

3.1. Validation of the model

To compare the flow distributions at different field flow rate, the dimensionless row flow rate was introduced. The dimensionless flow rate V_i' in the *i*-th collector row is defined by (Eq. 12) as:

$$V'_i = \frac{V_i}{(\sum_{i=1}^{N} V_i) \cdot A_{row,i}/A_{field}} \qquad \text{(Eq. 12)}$$

In (Eq. 12), V [m^3 h^{-1}] is the row flow rate, A [m^2] is the collector area, subscript i denotes the collector row number and N is the total number of collector rows. So, the dimensionless flow rate V'_i represents the ratio between the actual flow rate in the *i*-th collector row and the ideal flow rate in case of uniform distribution.

The measured and modeled flow distributions in terms of dimensionless flow rate are shown in Fig. 5. It is easy to recognize the effect that the change in first 10 valve settings had on flow distribution in the eastern subfield (rows 1-12) compared to the western subfield (rows 13-24). In the eastern subfield the row flow rates decreased progressively in the first 10 rows, only to return to their nominal value in the last two rows, whose valves were not changed. In the western subfield, where the valve settings were not modified, the row flow rates were much more similar to each other.

The agreement between model and measurements was evaluated through the root-mean-square deviation (*RMSD*) (Eq. 13).

$$RMSD = \sqrt{\frac{\sum_{i=1}^{N} (\hat{V}_i' - V_i')^2 \cdot b_i}{N}} \qquad \text{(Eq. 13)}$$

In (Eq. 13), V_i' [-] is the dimensionless form (Eq. 12) of measured flow rate in the *i*-th collector row in case of the model validation, while V_i'=1 in case of the investigated scenarios (Section 3.2); $\hat{V}_i'$ is the dimensionless form (Eq. 12) of modelled flow rate in the *i*-th collector row. The parameter b_i is a weight defined by (Eq. 14). If all rows are identical, *b*=1.

$$b_i = A_{row,i} / (A_{field}/N) \qquad \text{(Eq. 14)}$$

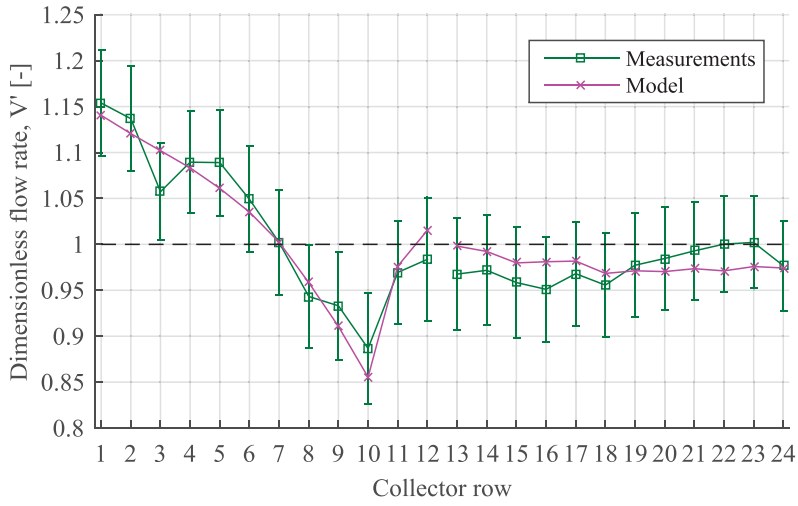

Fig. 5: Comparison between measured and modeled flow distribution for a field flow rate of 50.3 m^3 h^{-1}.

Measurements and model showed an overall good agreement, with a RMSD of 0.022. In the eastern subfield the measured and modeled flow distribution profiles had the same trend, except for the third row, characterized by the highest deviation between measurement and model. In fact, the measured flow rate was

significantly lower compared to the neighboring rows. This deviation was most likely caused by additional flow resistance in this collector row, maybe due to some obstruction or dirt clog. Also the original setting of its balancing valve was larger (and hence the valve more open) than the valve settings of neighboring rows. So, already when balancing the flow at the start-up phase of the collector field, it was noted that, in order for the third row to receive the design flow rate, its valve had to be opened more than expected.

3.2. Investigated scenarios

Using the developed model, the flow distribution across a solar collector field was evaluated in different scenarios. A 35% propylene glycol/water mixture was assumed as collector fluid and its fluid properties were evaluated through (Eq. 5-Eq. 7). The following scenarios were investigated:

- Case 1. The operating conditions used for the simulation were similar to those actually used in Høje Taastrup collector field. The inlet temperature was 55 °C and the solar irradiance on the collector plane was varied with the flow rate so that the outlet temperature was about 95 °C (Eq. 10). The same balancing valves settings as those used in Høje Taastrup collector field in normal operation were used in the model.
- Case 2. As shown by the experience of the first solar collector fields built in Sweden in 80'-90', good flow distribution can be achieved without balancing valves in case of collector array with regular geometry and constant diameter of the distribution pipes. To see the effect that a more complex geometry would have on the flow distribution in case of no balancing valves, the layout of the collector field was modified as shown in Fig. 6.a. The 24 rows were now connected all in parallel and they had a different number of collectors. Because in this case the collectors were 204 instead of 240 (case 1), the highest field flow rate was proportionally decreased from 50 m^3 h^{-1} to 42.5 m^3 h^{-1}. Two different subcases were considered. In case 2.2 the diameter of the supply and return pipes decreased as fluid was diverted to the collector rows. In case 2.1 the pipe diameter of the distribution pipes was kept constant and equal to 10.7 cm, i.e. the largest diameter in subcases 2.2. Pipes commercially available for this kind of application (Logstor, 2005) were used. The field inlet and outlet temperature was 50 °C and about 85 °C respectively.

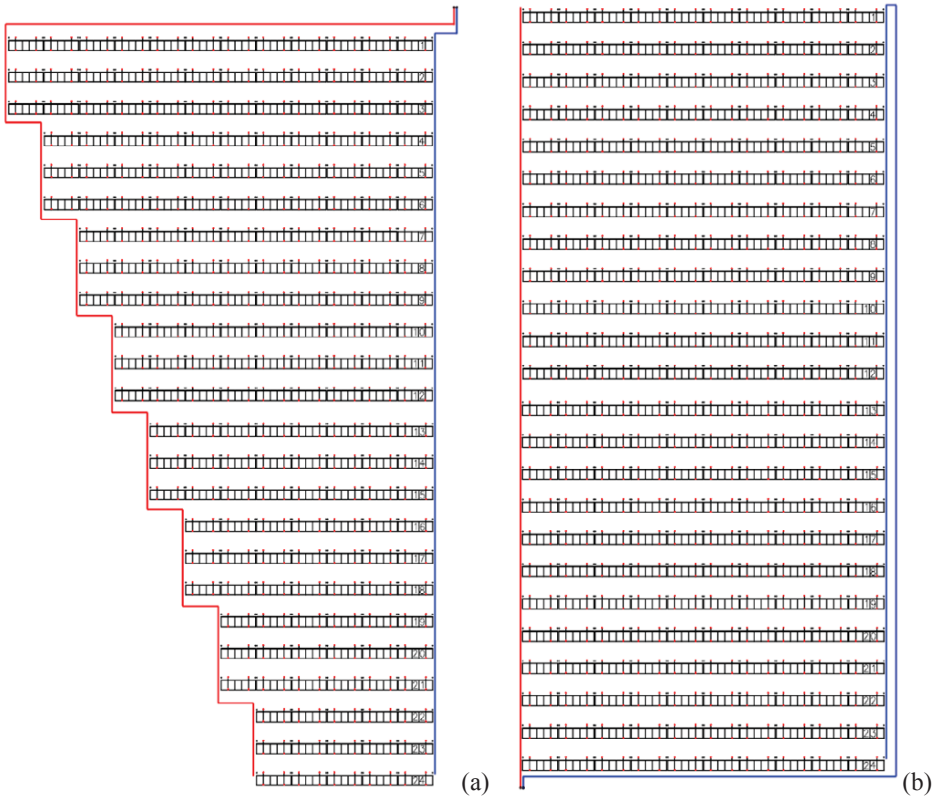

Fig. 6: Layout of the collector field assumed in case 2 (a) and in case 3 (b) (adapted from Arcon-Sunmark A/S).

- Case 3. This scenario used a Tichelmann connection (Fig. 6.b), which is expected to give a fairly uniform configuration due to the identical length for each hydraulic path. Hence, no valves were installed. As in case 2, two subcases were considered: case 3.1, having a constant pipe diameter of the distribution

pipe, and case 3.2, with decreasing pipe diameter according to the flow rate in each pipe segment. As in case 1, the inlet temperature was 55 °C and field outlet temperature was about 95 °C.

3.2.1. Case 1: normal operating conditions

The flow distribution in this case is shown in Fig. 7 for different field flow rates.

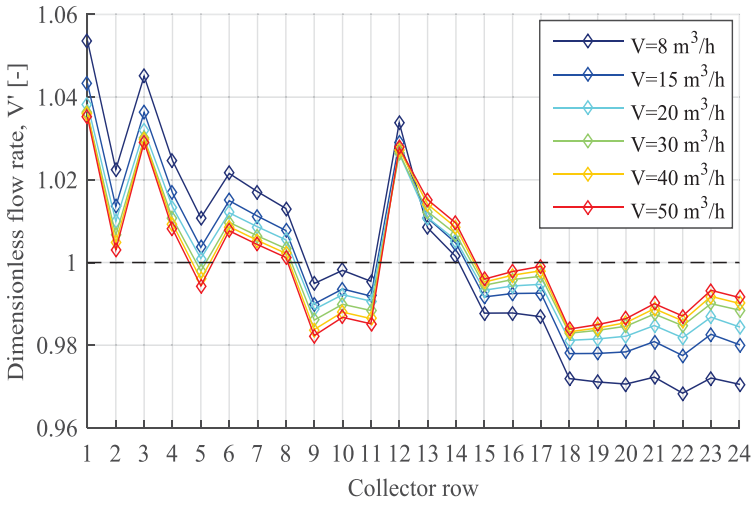

Fig. 7: Modeled flow distributions in Høje Taastrup solar collector field for different field flow rates, assuming normal operating conditions (case 1).

Also in the simulated scenarios the RMSD was used as the main parameter to quantify the level of maldistribution. Though, as no measurements were carried out for the simulated scenarios, the uniform distribution profile was now taken as term of comparison and hence z=1 in (Eq. 13) for any value of i.

Fig. 7 shows that the higher the flow rate, the more uniform the flow distribution. For $V \geq 30$ m^3 h^{-1}, the RMSD was approximately constant and equal to 0.015. At lower flow rates this value increased up to 0.025 for a flow rate of 8 m^3 h^{-1}. This was expected, as the balancing valves were set to give a uniform distribution at the nominal field flow rate, i.e. the highest flow rate the collector field operates at. The highest deviation between row flow rates and perfectly uniform flow distribution was lower than 6%, and the maximum difference between highest and lowest row flow rates was within 8%. Hence, the flow distribution can be considered acceptable for all the considered flow rates, as it differs from the ideal case less than 10%, which is considered the maximum acceptable deviation according to the German standard (VDI, 2004).

3.2.2. Case 2: Collector rows with different number of collectors

This scenario considered only cases where no balancing valves were installed, as these would give uniform flow distribution when properly regulated. The flow distribution in the two investigated subcases is shown in Fig. 8, with the subcase 2.1 characterized by much stronger maldistribution than subcase 2.2.

Given the field layout (Fig. 6.a), the collector rows became shorter while getting farther away from the pumping station. As the collector row represented the main contribution in terms of pressure drop along a hydraulic path, rows with fewer collectors had a much lower hydraulic resistance. So, in absence of balancing valves, these rows diverted flow rates higher than their design value. In case of constant pipe diameter in the distribution pipes (case 2.1) the flow maldistribution was higher with the RMSD ranging between 0.40-0.43 depending on the flow rate. The maximum deviation occurred in the last three rows, with flow rates about twice as high as the nominal value. The distribution was not very uniform, but still considerably better, in case 2.2, where the diameter was progressively decreased. In this case, the maximum deviation was only 40% and the RMSD was in the range 0.18-0.20. In fact, in case of constant diameter the fluid velocity progressively decreased in the pipe segments, making their contribution to the pressure drop of the entire hydraulic path very small. In order for all hydraulic paths to give the same pressure drop, the flow rate in the rows with fewer collectors had to increase significantly. Conversely, decreasing the pipe diameter gave similar pressure gradient in the different pipe segments. This increased the resistance of the hydraulic

paths of the collector rows which lay farther away, resulting in a more uniform flow distribution.

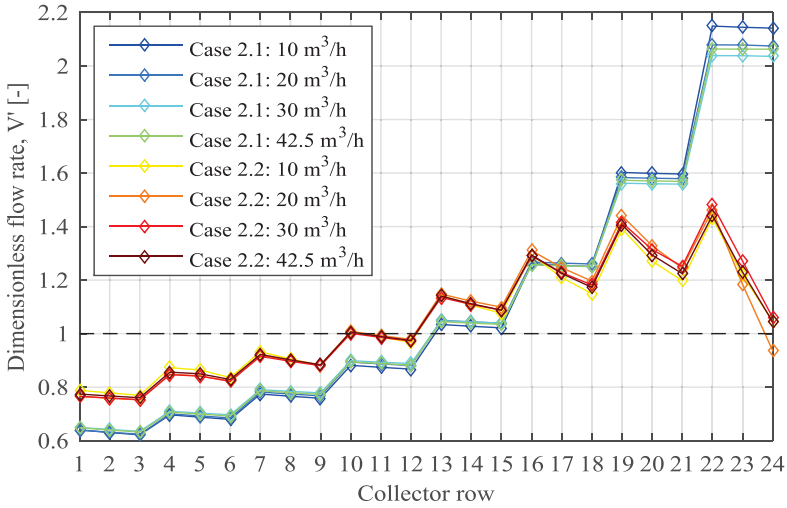

Fig. 8: Modeled flow distributions for different field flow rates in case 2.

3.2.3. Case 3: Tichelmann connection

Fig. 9 shows the flow distribution in the subcases 3.1 and 3.2. For sake of clarity, for each subcase only two flow rates, which gave the most and least uniform distribution, are shown. In both scenarios the Tichelmann connection assured a good flow distribution with deviations from the perfectly uniform case no larger than 4%. Subcase 3.2 achieved a slightly better distribution (RMSD=0.008-0.010) compared to subcase 3.1 (RMSD=0.014-0.016). In the latter, the choice of keeping a constant pipe diameter resulted into a U-shape flow distribution profile. In fact, although the pipe length was the same for each hydraulic path, the paths in more central position (rows 9-13) were supplied with lower flow rates. This was due to the fact that these paths included distribution pipes segments with higher flow rates (and hence higher pressure drop) compared to the more peripheral paths. In subcase 3.2 the distribution pipe diameter was progressively varied, so that the fluid velocity was similar in all pipe segments. This resulted in similar pressure drops and hence a more uniform flow distribution. Varying the pipe diameter also saved pipe material (steel and insulation), reducing cost and thermal losses. The main drawback of a Tichelmann connection is the longer pipe length.

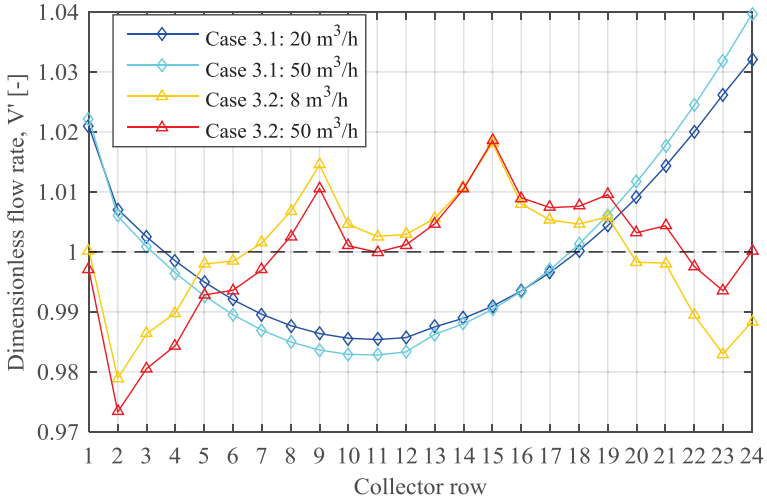

Fig. 9: Modeled flow distributions for different field flow rates in case 3.

3.3. Effect of the flow maldistribution on the thermal performance of the collector field

Modifying the row composition of the collector field shown in Fig. 6.a, different degrees of flow maldistribution were caused. The effect on the power output of the collector field is shown in Fig. 10 for two collector types, a HTHEATStore 35/08 (SP, 2016a) (Section 2.1.1) and a HTHEATBoost 35/08 (SP, 2016b)

(η_0=0.786, a_1=2.97 W m^{-2} K^{-1} and a_2=0.009 W m^{-2} K^{-2}). The collectors differed only for the presence of a polymer foil, working as convection barrier, between glass cover and absorber in the HTHEATBoost model. The loss in power output was calculated with respect to the case where the collector row flow rates were exactly proportional to the collector row area. The power output, P_{out} [W], was calculated through (Eq. 15):

$$P_{out} = \sum_{i=1}^{N} \left(\dot{m}_i \cdot c_{p,i}(\bar{T}_i) \cdot \left(T_{out,i} - T_{in} \right) \right) \qquad \text{(Eq. 15)}$$

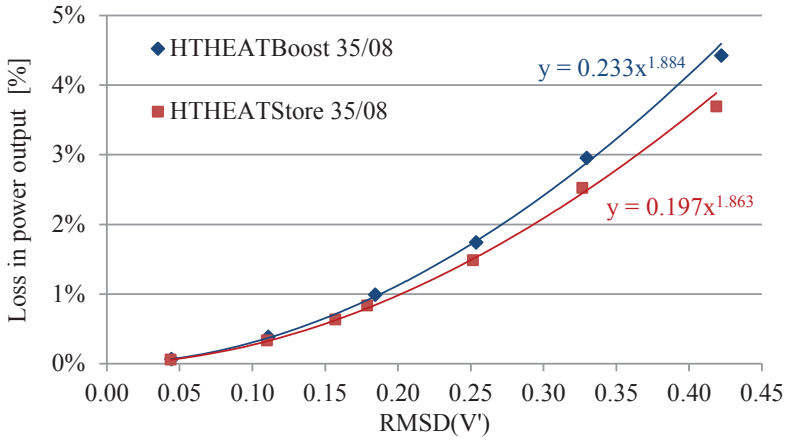

Fig. 10: Maximum reduction in power output of a solar collector field as function of the flow maldistribution.

It can be seen that the reduction in power output is proportional to the RMSD of the flow distribution to the 1.9th power, very similar to the result of Chiou (1982) for a single collector (Section 1.1). The loss in power output is relatively small, within 5% for RMSDs up to 0.4. However, it should be noted that in the current study pipe losses were neglected and the collector efficiency was assumed independent of the collector flow rate. In reality, lower efficiency is expected at low flow rates, especially if these cause laminar regime in the absorber pipes (Bava and Furbo, 2014). Slightly stronger effect on the power output would result, if these aspects were taken into account too. As expected, the performance of the collector field made of HTHEATBoost modules was more affected by the flow maldistribution. In fact, given the higher heat loss coefficients of this collector, its efficiency was more penalized in those rows which were supplied with lower flow rates and hence reached unnecessarily higher temperatures.

4. Conclusions

A model for calculating the flow distribution in a solar collector field was developed. The model results were compared against measurements and a good agreement was found.

The model was used to study different scenarios. Balancing valves in each collector row guaranteed good flow distribution in all the operating conditions. Although the valves were set in full load conditions, the deviations occurring at different operating conditions were still within the range of ±10%.

A Tichelmann connection gave a good flow distribution also without balancing valves. Reducing the pipe diameter of the distribution pipes was a good measure to improve the distribution and decrease the pipe cost.

In case of irregular field layout with collector rows having a different number of modules, balancing valves seemed to be the only way to reach uniform flow distribution.

5. Acknowledgements

The authors are thankful to the Marie-Curie Actions - Initial Training Network research programme of the European Union which supported the first author through the SolNet-SHINE project. The authors are also grateful to the company Arcon-Sunmark A/S and the DH company Høje Taastrup Fjernvarme for providing useful information necessary to develop the model and for granting access to the solar collector field.

6. References

Bava, F., Furbo, S., 2016. A numerical model for pressure drop and flow distribution in a solar collector with horizontal U-connected pipes. Solar Energy 134, 264–272.

Chiou, J.P., 1982. The effect of nonuniform fluid flow distribution on the thermal performance of solar collector. Solar Energy 29, 487–502.

Conde, M., 2011. Thermophysical properties of brines – Models, Conde Engineering, Zurich.

DOW, 2008. Engineering and Operating Guide for DOWFROST and DOWFROST HD Inhibited Propylene Glycol-based Heat Transfer Fluids.

EnergySupply, 2016. Danmarks største solenergianlæg. http://www.energy-supply.dk/article/view/235192/.

Fan, J., Shah, L.J., Furbo, S., 2007. Flow distribution in a solar collector panel with horizontally inclined absorber strips. Sol. Energy 81, 1501–1511.

Furbo, S., Perers, B., Bava, F., 2015. Thermal performance of solar district heating plants in Denmark, in: Conference Proceedings of EuroSun 2014. Aix-les-Bains (France).

George, J., Sastry, N. V., 2003. Densities, Dynamic Viscosities, Speeds of Sound, and Relative Permittivities for Water + Alkanediols (Propane-1,2- and -1,3-diol and Butane-1,2-, -1,3-, -1,4-, and -2,3-Diol) at different Temperatures. Journal of Chemical and Engineering Data 48, 1529–1539.

Haaland, S.E., 1983. Simple and Explicit Formulas for the Friction Factor in Turbulent Flow. Journal of Fluids Engineering (ASME) 105, 89–90.

Holman, J.P., 2002. Heat transfer, 9th ed. McGraw-Hill, New York.

Idelchik, I.E., 1994. Handbook of hydraulic resistance, 3rd ed. CRC press, Boca Raton.

IMI Hydronic, 2015. STAD Balancing valves DN 15-50. IMI Hydronic Engineering. Online at http://www.imi-hydronic.com/en/products-solutions/balancing-and-control/balancing-valves/.

IMI Hydronic, 2014. HySelect User Manual. IMI Hydronic Engineering. Online at http://www.imi-hydronic.com/en/knowledge-tools/hydronic-tools-software/balance-control/ta-select-4/.

Knabl, S., Fink, C., Ohnewein, P., Mauthner, F., Hausner, R., 2014. Requirements and guidelines for collector loop installation, Deliverables of IEA-SHC Task 45 Large scale solar heating and cooling systems. Online at http://task45.iea-shc.org/fact-sheets.

Mauthner, F., Weiss, W., Spörk-Dür, M., 2016. Solar Heat Worldwide. Markets and Contributions to the Energy Supply 2014. Online at http://www.iea-shc.org/solar-heat-worldwide.

Melinder, Å., 2007. Thermophysical Properties of Aqueous Solutions Used as Secondary Working Fluids. Royal Institute of Technology, KTH.

Rohde, J.E., Knoll, R.H., 1976. Analysis of a solar collector field water flow network. Lewis Research Center, Cleveland (Ohio, USA).

SP - Technical Research Institute of Sweden, 2016a. Solar Keymark Certificate No. SP SC0842-14: HTHEATstore 35/08 . Borås (Sweden). Online at http://www.solarkeymark.dk/.

SP - Technical Research Institute of Sweden, 2016b. Solar Keymark Certificate No. SP SC0840-14: HTHEATboost 35/08 . Borås (Sweden). Online at http://www.solarkeymark.dk/.

VDI, 2004. VDI-Richtlinie: VDI 6002 Blatt 1 Solare Trinkwassererwärmung - Allgemeine Grundlagen - Systemtechnik und Anwendung im Wohnungsbau.

Wang, X.A., Wu, L.G., 1990. Analysis and performance of flat-plate solar collector arrays. Solar Energy 45, 71–78.

Windeleff, J., Nielsen, J.E., 2014. Solar District Heating in Denmark.